# AN OPTICAL STREAKING METHOD FOR MEASURING FEMTOSECOND ELECTRON BUNCHES

Yuantao Ding, Karl L. F. Bane and Zhirong Huang, SLAC, Menlo Park,CA, USA

*Abstract*

The measurement of the ultra-short electron bunch length on the femtosecond time scale constitutes a very challenging problem. In the x-ray free electron laser facilities such as the Linac Coherent Light Source, generation of a sub-ten femtoseconds electron beam with 20pC charge is possible, but direct measurements are very difficult due to the resolution limit of the present diagnostics. We propose a new method here based on the measurement of the electron beam energy modulation induced from laser-electron interaction in a short wiggler. A typical optical streaking method requires a laser wavelength much longer than the electron bunch length. In this paper a laser with its wavelength shorter than the electron bunch length has been adopted, while the slope on the laser intensity envelope is used to distinguish the different periods. With this technique it is possible to reconstruct the bunch longitudinal profile from a single shot measurement.

## INTRODUCTION

Generation of ultrashort x-ray pulses at femtoseconds (fs) scale is of great interest within synchrotron radiation and free electron laser (FEL) user community. One of the simple methods is to operate the FEL facility at low charge. At the Linac Coherent Light Source (LCLS), we have demonstrated the capability of generating ultrashort electron-beam (e-beam) with a duration of less than 10 fs fwhm using 20 pC charge [1, 2]. The x-ray pulses have been delivered to the x-ray users with a similar or even shorter pulse duration. However, The measurement of such short electron or x-ray pulse length at the fs time-scale constitutes a challenging problem.

A standard method using an S-band radio-frequency (rf) transverse deflector has been established at LCLS, which works like a streak camera for electrons and is capable of resolving bunch lengths as short as 25 fs fwhm [1]. With this device, the electrons are transversely deflected by the high-frequency time-variation of the deflecting fields. Increasing the deflecting voltage and rf frequency are the right direction to achieve a better resolution. For example, by choosing an X-band transverse deflecting cavity, the expected resolution for LCLS beam with 4.3 GeV is about 1 fs rms [3]. Typically the rf breakdown threshold and the power source availability prevent going to even higher voltage and frequency.

With the highly-developed laser techniques, we can choose to streak the beam at optical frequencies. By jumping from rf to optical frequency, the wavelength is shortening by 4 to 5 orders. With an electron bunch length shorter than half period of the laser, we can apply the similar rf deflecting or zero-phasing method for e-beam bunch length measurements using a high-power laser. A short wiggler is required to provide interaction between the electron and the laser. For example, to measure the e-beam at the order of 1 m rms length, a laser with its wavelength of 10 $\mu$m may be considered. For a typical few GeV e-beam, the wiggler period has to be large to satisfy the resonance condition. Also, if the e-beam is longer than one laser period, the different modulation periods will overlap and we cannot distinguish them. So this method is so far limited by the achievable long-wavelength laser power. To get an effective modulation on an e-beam of 4.3 GeV, the required laser power is about a few tens GW.

In this paper we propose to adopt a high-power Ti:Sapphire laser (wavelength of 800 nm), and use the slope in the intensity envelope to distinguish the different modulation periods. First an ultrashort electron beam interacts with the Ti:Sapphire laser in a wiggler, where the electron energy is modulated at the same periods of the laser. If the laser pulse is long and the short electron bunch is overlapped (in time) with the middle part of the laser, such as the setup at LCLS laser heater, the different energy modulation periods on the electron beam will be overlapped on the energy profile. In this condition we typically have a double-horn distribution of the energy profile [4], and the electron-bunch length information cannot be retrieved. But if the laser pulse (with a Gaussian temporal shape) is relatively short, we can synchronize the e-beam with the laser at the slope region of the intensity envelope, and the amplitude of each energy modulation period will be different. Then these electrons pass through a dispersive section such as a spectrometer, after that this periodically-modulated energy profile can be observed in a transverse screen. By properly choosing the laser parameters, each modulation period will show as a separate streak on the screen. This modulation period in energy dimension correlates to the laser wavelength in time dimension. Since the laser wavelength is a known parameter, no additional calibration is needed. This provides a single shot, self-calibrated method for ultrashort electron bunch length measurements.

## LASER ELECTRON INTERACTION IN A WIGGLER

We first describe an analytical model on the laser electron interaction in a short wiggler, similarly in the way de-

ISBN 978-3-95450-117-5

veloped in [5]. Here we assume a Gaussian temporal envelope with an intensity rms pulse length of $\sigma_s$. The laser electric field at fundamental Gaussian mode can be written as

$$\vec{E}(z,t) = \vec{e_x}\frac{E_0}{\sqrt{1+z^2/z_R^2}}\cos(kz-\omega t+\phi(r,z)) \times e^{-r^2/w^2(z)}e^{-s^2/4\sigma_s^2}, \quad (1)$$

where

$$\begin{aligned}\phi(r,z) &= -\arctan\frac{z}{z_R}+\frac{kr^2z}{2(z^2+z_R^2)}+ks+\phi_0,\\ k &= 2\pi/\lambda,\\ z_R &= \frac{\pi w_0^2}{\lambda} = kw_0^2/2,\\ w^2(z) &= w_0^2(1+z^2/z_R^2), w_0 = 2\sigma_{r0},\\ r^2 &= x^2+y^2,\end{aligned} \quad (2)$$

Note $w_0$ is in terms of laser intensity here, which is $\sqrt{2}$ smaller than that for the laser field amplitude. For the electrons wiggling in the horizontal plane of a planar wiggler, we can write the velocity in $x$ dimension as:

$$\vec{v_x} = \vec{e_x}\frac{Kc}{\gamma}\cos(k_u z). \quad (3)$$

So the energy exchange of the laser and the electrons in a wiggler is:

$$mc^2\frac{d\gamma_L}{dt} = e\vec{E}\cdot\vec{v_x} = \frac{eE_0kc}{\gamma}\frac{1}{\sqrt{1+z^2/z_R^2}} \times\cos(kz-\omega t+\phi(r,z))\cos(k_uz)e^{-r^2/w^2(z)}e^{-s^2/4\sigma_s^2}. \quad (4)$$

We can define the following parameters for convenience as:

$$\begin{aligned}\bar{z} &= \frac{z}{N\lambda_u}, t = z/c,\\ q &= \frac{N\lambda_u}{z_R},\\ \nu &= \frac{2N\Delta\gamma}{\gamma}, \Delta\gamma = \gamma-\gamma_r.\end{aligned} \quad (5)$$

where $\gamma_r$ is the FEL resonance energy, with $\gamma_r^2 = \frac{k}{2k_u}(1+K^2/2)$. Note $z/z_R = q\bar{z}$, which is useful in the following analysis. Using a generation function for Bessel functions and also by averaging over one wiggler period we can get the electrons energy loss $G$ along the undulator $\bar{z}$ from Eq. (4):

$$G = \frac{d\gamma_L(r,s)}{d\bar{z}} = \frac{A_0}{\sqrt{1+(q\bar{z})^2}}\cos\psi e^{-\frac{r^2}{w^2(z)}}e^{\frac{-s^2}{4\sigma_s^2}}, \quad (6)$$

where $A_0 = \sqrt{\frac{P_L}{P_0}}\frac{2KL_w}{\gamma w_0}$[JJ], $\psi = 2\pi\nu\bar{z}-\arctan(q\bar{z})+ks+\frac{kr^2(q\bar{z})^2}{2\bar{z}N\lambda_u(1+(q\bar{z})^2)}+\phi_0$, and [JJ] $= J_0(\xi/2)-J_1(\xi)$ with $\xi = K^2/(2+K^2)$.

By integrating Eq. (6) along the undulator distance, we get the energy change at the end of the wiggler:

$$\Delta\gamma_L(r,s) = \int_{-0.5}^{0.5}d\bar{z}G. \quad (7)$$

The electron distribution is modified due to the laser-electron interaction. Assuming initially Gaussian distributions in energy and in transverse coordinates, the electron distribution function, including the transverse and temporal dependence, becomes

$$f_0(s,\Delta\gamma_0,r) = \frac{I_0}{ec\sqrt{2\pi}\sigma_{\gamma_0}}\exp\left\{-\frac{[\Delta\gamma_0-\Delta\gamma_L(r,s)]}{2\sigma_{\gamma_0}^2}\right\} \times\frac{1}{2\pi\sigma_x^2}\exp\left(-\frac{r^2}{2\sigma_x^2}\right), \quad (8)$$

where $\sigma_{\gamma_0}$ is the initial uncorrelated energy spread, and $\sigma_x(=\sigma_y)$ is the rms electron beam size in the transverse plane. Integrating this distribution function over transverse and longitudinal coordinates, we obtain the modified energy distribution

$$V(\Delta\gamma_0) = 2\pi\int rdr\int dsf_0(s,\Delta\gamma_0,r). \quad (9)$$

We can simplify Eq. (6) and (7) with assuming a large laser rayleigh length ($q=0$), then the energy change is :

$$\Delta\gamma_L(r,s) = A_0\cos(ks)e^{-\frac{r^2}{w_0^2}}e^{\frac{-s^2}{4\sigma_s^2}}. \quad (10)$$

This equation is similar with Eq. (8) in reference [4], but adding a longitudinal Gaussian distribution term here.

## SYSTEM LAYOUT AND PARAMETERS

A schematic layout of the diagnostics system is shown in Fig. 1. The electron beam interacts with an optical laser in a short wiggler, and the modulated energy distribution is measured downstream through an energy spectrometer. We pick up the electron parameters of LCLS after the second bunch compressor, where the electron energy is 4.3 GeV. We use a Ti:sapphire laser with $\lambda = 0.8\mu m$, the wiggler period $\lambda_u$ is 0.25 m and the period number $N = 10$. The main electron and laser parameters are summarized in Table 1.

## NUMERICAL SIMULATIONS

Elegant [6] is used to simulate the laser electron interaction and track the beam down to the spectrometer screen. In the simulations, we choose an ideal electron bunch of 3 fs rms with a typical linear energy chirp to demonstrate this method. The uncorrelated energy spread of the initial beam is 1 MeV rms. The initial longitudinal phase space and current profile are shown in Fig. 2(a) and 2(b). The laser duration is 50fs fwhm in intensity, with a peak power of 1 TW.



ISBN 978-3-95450-117-5

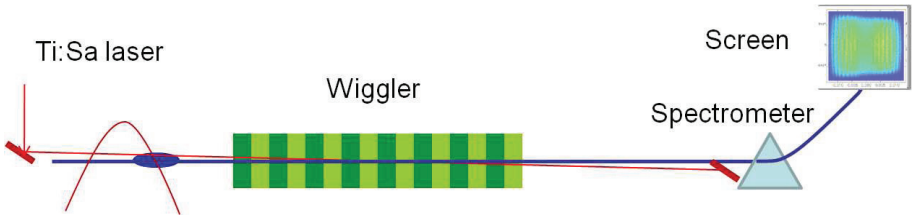


Figure 1: The schematic layout of the diagnostic system.

Table 1: Main Parameters for the System

| Parameter | Symbol | Value | Unit |
|---|---|---|---|
| Electron energy | E | 4.3 | GeV |
| rms emittance | $\gamma\varepsilon$ | 0.5 | $\mu$m |
| rms duration | $\sigma_t$ | 3 | fs |
| rms energy spread | $\sigma_E$ | 1 | MeV |
| Laser wavelength | $\lambda$ | 800 | nm |
| peak power | $P_L$ | 1 | TW |
| pulse duration (fwhm) | $\Delta t$ | 50 | fs |
| waist size | $w_0$ | 350 | $\mu$m |
| Wiggler period | $\lambda_u$ | 0.25 | m |
| period number | N | 10 | |
| spectrometer dispersion | $\eta$ | -0.89 | m |

We synchronize the electron with the laser intensity peak by an offset of 45 fs. After the laser-electron interaction in the wiggler, the longitudinal phase space and energy profile are shown in Fig. 2(c) and 2(d). We can see that the energy distribution is asymmetric, which is due to the initial energy chirp in the bunch. This linear chirp enhances the energy modulation amplitude on one side but suppresses on the other side. The energy profile in Fig. 2(d) clearly shows the spikes modulated from the different laser periods.

After passing through a horizontal dispersive section, we observe the transverse beam distribution on the screen which is shown in Fig. 3(a). The horizontal dimension represents the energy, and we can see that its projection (Fig. 3(b)) gives the same profile shape as that from Fig. 2(d). We remove the background by fitting the spikes and obtain the residual of the modulation (Fig. 3(c)). In this example the different modulation periods are clearly distinguished and the distance between two adjacent peaks is one laser period. Then we take the peaks from the residual plot and rescale the horizontal axis using laser wavelength, and fit the peaks to get the bunch length, as shown in Fig. 3(d). The fitting result is 2.9 fs rms (comparing with the original length of 3 fs rms) and the bunch temporal shape is also determined.

As mentioned above, the asymmetric distribution of the horizontal profile (see Fig. 3(b)) is due to the initial time-energy chirp. Since we know the dispersion $\eta$ of the spectrometer, the energy distribution can be obtained from $\delta = x/\eta$. If the chirp is small compared with the slope of the laser envelope, it is also possible to resolve the image streaks on both sides. under this condition, the horizontal

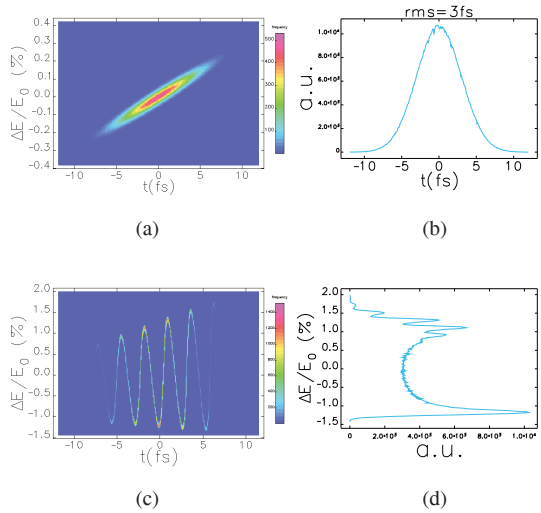


(a) (b) (c) (d)

Figure 2: The initial electron longitudinal phase space (a) and current profile (b) before the wiggler. After laser-electron interaction, the electron longitudinal phase space (c) and energy profile (d).

difference of the two adjacent peaks between the two sides gives the initial beam time-energy chirp. For example, if the measured period lengths from the two sides are $\Delta x_1$ and $\Delta x_2$, then the initial chirp is given

$$h = \frac{\Delta x_1 - \Delta x_2}{\eta \Delta t}, \tag{11}$$

where $\Delta t = \lambda/c$.

Figure 4 shows an example to analyze the initial time-energy chirp of the e-beam. This is the same e-beam in Fig. 2(a), but we increased laser power to 4 TW. With this laser power, both sides of the periodic modulation on the energy profile can be determined. As seen from the figures, after plotting the horizontal peaks versus time we can see the different slope which can be used to analyze the chirp based on Eq. (11). The analyzed chirp in this example is 0.0011/11fs, which is same as the initial beam (chirp is 1e-4/fs). If one side of the energy profile is smeared together due to limited laser power, it is also possible to roughly estimate the initial beam chirp by comparing the full widths at the half maximum from the two sides of the the smoothed profile.

ISBN 978-3-95450-117-5

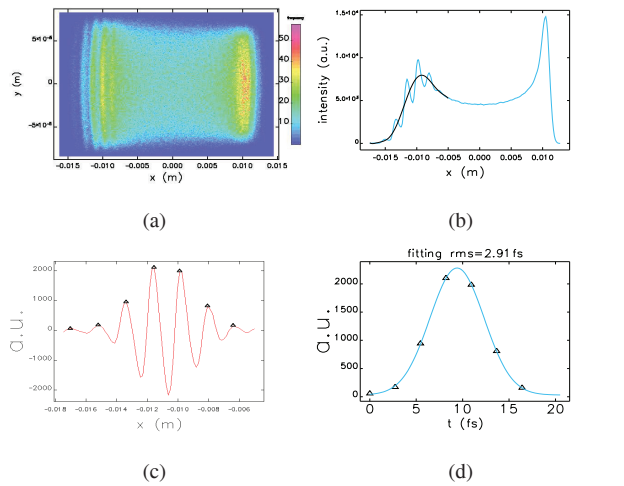


Figure 3: The transverse image on the screen (a) and its horizontal projection (b). After removing the background by fitting a black curve in (b), the residual is shown in (c). The peak points are replotted in (d) using laser wavelength to calibrate the horizontal axis.

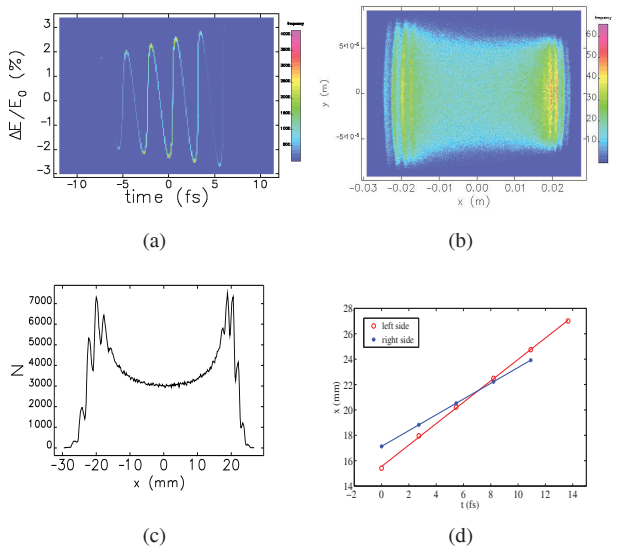


Figure 4: The electron longitudinal phase space right after the wiggler (a) and the transverse image at the screen after the spectrometer (b). The horizontal profile in (c) shows the difference between the left and right sides. The different slope shown in (d) is used to analyze the initial e-beam chirp.

## DISCUSSIONS

As shown from the simulation examples, if the difference of the energy modulation amplitude between two adjacent periods is larger than the e-beam intrinsic slice energy spread, then it is possible to distinguish the different modulation periods, which can be further measured after an energy spectrometer. Once the different streaks have been resolved, we only have to count the number of the streaks to know the electron bunch length. In addition, by fitting to remove the background, the e-beam temporal profile shape can also be determined. Since one step is one laser wavelength, this determines the resolution limit.

Since we require the e-beam interacts with the laser at the slope region, the timing between the laser system and the e-beam is important. With the parameters listed in Table 1, an offset of 10 fs is still acceptable for the profile reconstruction. The present LCLS e-beam time arrival jitter is about 50 fs rms [1]. Together with the optical laser system, if we assume the jitter between the laser and the e-beam is 100fs rms [7], roughly there are about 10% bunches which have the chances to meet at the linear slope regime.

There are some tricks to increase the slope of the laser intensity envelope. For example, using the beating mode with two frequencies to form a stronger slope of the intensity envelope. The nonlinearity of the laser slope and the initial e-beam time-energy chirp makes additional measurement errors.

We also tested this method with the LCLS Start-to-end simulated beam at 20 pC. At over-compression mode with a Gaussian-like shape, after reconstruction we achieve a pretty good agreement; at the under-compression mode with a double-horn shape, since there are only a few points, the double-horn shape can not be retrieved due to the resolution limit, but at least we get some upper limit of the e-beam bunch length.

## REFERENCES

[1] P. Emma *et al.*, Nat. Photon. **4**, 641 (2010).

[2] Y. Ding *et al.*, Phys. Rev. Lett, **102**, 254801 (2009).

[3] Y. Ding *et al.*, WEPA01, this FEL2011 conference.

[4] Z. Huang *et al.*, Phys. Rev. ST Accel. Beams **7**, 074401 (2004)

[5] A.A. Zholents and M.S. Zolotorev, New Journal of Physics, **10**, 025005 (2008).

[6] M. Borland, *Elegant*, Advanced Photon Source LS-287, 2000.

[7] A. Brachmann *et al.*, IPAC10; see also SLAC-PUB-14234.



ISBN 978-3-95450-117-5